

# Silicon waveguides for the mid-infrared wavelength region

G. Z. Mashanovich<sup>a\*</sup>, S. Stankovic<sup>b</sup>, P. Y. Yang<sup>a</sup>, E. J. Teo<sup>c</sup>, F. Dell'Olio<sup>d</sup>,  
V. M. N. Passaro<sup>d</sup>, A. A. Bettiol<sup>c</sup>, M. B. H. Breese<sup>c</sup>, G. T. Reed<sup>a</sup>

<sup>a</sup> Advanced Technology Institute, University of Surrey, Guildford, GU2 7XH, UK

<sup>b</sup> Faculty of Electrical Engineering, University of Belgrade, 11120 Belgrade, Serbia

<sup>c</sup> Department of Physics, 2 Science Drive 3, National University of Singapore, 117542 Singapore

<sup>d</sup> Dipartimento di Elettronica, Politecnico di Bari, Via E. Orabona 4, 70125 Bari, Italy

## ABSTRACT

Mid-infrared wavelength region is interesting for several application areas including sensing, communications, signal processing, and imaging. Its importance stems from the two atmospheric windows and the fact that nearly all important molecular gases have strong absorption lines in the mid-infrared. In this paper, we discuss the design, fabrication and propagation loss measurements of three silicon waveguide structures that can find applications in the mid-infrared region.

**Keywords:** Silicon photonics, mid-infrared, optical waveguides, silicon on insulator

## 1. INTRODUCTION

The vast majority of research effort in Silicon Photonics is focused on the 1.55  $\mu\text{m}$  wavelength band. However, the mid-infrared (MIR) spectral region is of enormous interest as the practical realisation of optoelectronics devices operating in this wavelength range offers potential applications in a wide variety of areas including: optical sensing and environmental monitoring, free-space communications, biomedical and thermal imaging, infrared counter-measures. Many pollutant and toxic gases and liquids that we wish to detect or monitor exhibit bands of absorption lines in the infrared part of the spectrum. Consequently, the mid-infrared is very attractive for the development of sensitive optical sensor instrumentation. In addition there are two atmospheric transmission windows (3-5  $\mu\text{m}$  and 8-14  $\mu\text{m}$ ) which enable free space optical communications. Of interest are also thermal imaging applications in both civil and military situations as well as the development of infrared countermeasures for so called "homeland security". The mid-infrared photonics also offers extensive potential for development of minimally invasive, effective and safe diagnostic techniques. This spectral range is attractive for highly precise surgical procedures and medical ablation of tissue because of its high absorption in water, and hence small penetration depths, especially for wavelengths around 3  $\mu\text{m}$  where the penetration depth can be as small as a few microns [1]. However, the advantages of this wavelength range have not been fully exploited due to the limitations in current technology. The potential of this wavelength range is being pursued, via research in the MIR sources and detectors based on III-V materials, particularly on quantum cascade lasers and detectors (e.g. [2], [3]) and quantum well and quantum dot lasers and detectors (e.g. [4]). Nevertheless, relatively little results have been published on MIR silicon photonics.

The main challenge in migration to the MIR silicon photonics is that the basic building block of the photonic circuit, the optical waveguide, and materials for this wavelength range are not known. Silicon has two low-loss transmission windows, one from 1.2 to 6.6  $\mu\text{m}$  and the other from 24 to 100  $\mu\text{m}$  [5]. However,  $\text{SiO}_2$  is very lossy in the 2.6-2.9  $\mu\text{m}$  range and beyond 3.6  $\mu\text{m}$  [6]. Soref et al., have proposed several waveguide structures suitable for mid- and long-IR spectral regions [7]. In this paper, we discuss the design and fabrication of three candidate MIR waveguide structures, the hollow core, slot and waveguides with air or porous silicon claddings. For slot and hollow waveguides we have chosen a wavelength of 3.39  $\mu\text{m}$  in the design stage, firstly because that wavelength is interesting for sensing applications, and secondly because a Raman amplification has been recently reported at this wavelength [8].

---

\*g.mashanovich@surrey.ac.uk; phone +44 (0)1483 686123; fax + 44 (0)1483 689404

## 2. HOLLOW CORE WAVEGUIDES

Conventional optical waveguides suffer from shortcomings related to the propagation of light through a solid medium, such as dispersion and temperature dependence of the refractive index. In order to avoid these problems, hollow-core waveguides have been proposed (e.g. [9], [10]). The hollow-core waveguides have an air-filled core surrounded by a solid cladding comprised of the multilayer coating, designed to confine the propagating optical signal within the core (Fig. 1). As the light propagates through the air, there is virtually no dispersion nor problems with temperature dependence of the refractive index. Hollow-core waveguides can be also very useful for sensing applications as their core can be filled with gases or liquids, which is particularly interesting for the MIR as a number of gasses have absorption peaks in this range. Other potential applications of these waveguides include tight turning radii and high power transmission. Depending on the structure of the cladding, these waveguides are classified in two categories: the Bragg-mirror cladding waveguides and the ARROW (anti-resonant reflecting optical waveguide). The Bragg-mirror cladding comprises alternating layers of two types of materials, the so called “bilayers”. In this case, light is totally reflected at the multilayer, for any incident angle or polarisation and the light can propagate through a low refractive index core.

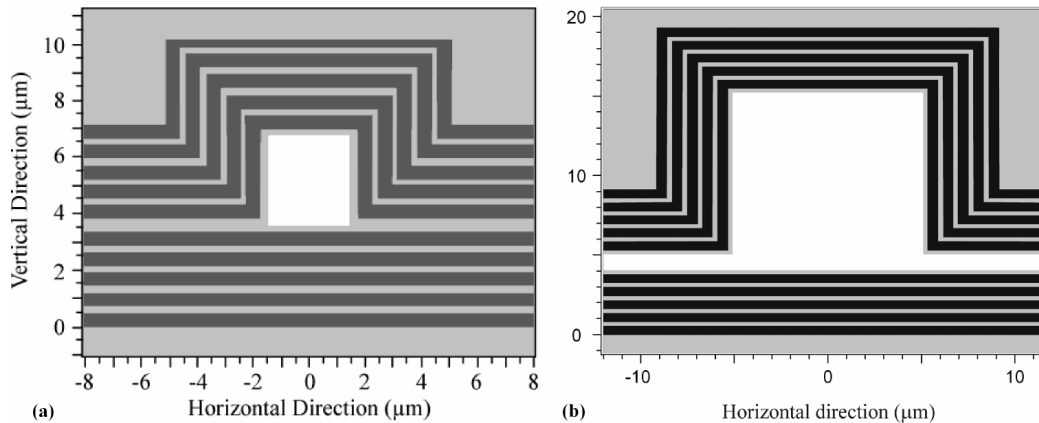


Fig. 1: Bragg type hollow waveguide a) without a gap between the two bonded wafers, b) with the gap

In this section we analyse hollow-core waveguides with the Bragg-mirror cladding (Fig 1), optimised for the wavelength of  $3.39 \mu\text{m}$ . We compare hollow core waveguides with two different claddings  $\text{Si}/\text{SiO}_2$  and  $\text{Si}/\text{Si}_3\text{N}_4$ . Specifically, we chose waveguides with the square core cross-section, as shown in Fig 1a. Such waveguides are comprised of the upper and the lower Bragg claddings fabricated on two silicon wafers which are subsequently bonded thus forming the hollow core in the middle. Due to a large difference in the refractive indices of  $\text{Si}$  and  $\text{SiO}_2$ , small propagation losses can be achieved with the waveguides having no more than 5  $\text{Si}/\text{SiO}_2$  bilayers in the cladding as can be seen in Table 1. We have used a 3-D beam propagation method [11] to calculate waveguide propagation losses for several different values of the core dimensions and overall number of bilayers in the cladding. For a better comparison, core dimensions (width and height) are expressed as multiples of the wavelength.

Although hollow core waveguides with a  $\text{Si}/\text{Si}_3\text{N}_4$  cladding has a broader spectral operation range than the waveguide with a  $\text{Si}/\text{SiO}_2$  cladding as  $\text{SiO}_2$  is more lossy than  $\text{Si}_3\text{N}_4$  in the mid-IR range, a lower refractive index contrast between  $\text{Si}$  and  $\text{Si}_3\text{N}_4$  results in higher propagation losses at  $3.39 \mu\text{m}$  for the same number of bilayers. Our simulations show that waveguides with only 4 or 5 bilayers in the cladding, yet with relatively large core dimensions of no less than three wavelengths in both width and height could exhibit propagation losses of less than 1 dB/cm.

The analysis was carried out for the ideal geometrical properties of the proposed square-shaped, hollow-core waveguides with Bragg-mirror claddings. Having in mind the fabrication procedure for such devices, this specific geometrical shape of the waveguide is difficult to produce. The process of fabrication would include making a trench in a silicon substrate, depositing alternating layers of  $\text{SiO}_2$  or  $\text{Si}_3\text{N}_4$  and  $\text{Si}$  and then back-bonding another wafer with the

deposited Bragg-mirror layers to eventually form a hollow-core waveguide with the square cross-section, as shown in Fig 1a. However, it is reasonable to expect that these two bonded wafers would form a gap at the interface. This gap would result in a waveguide cross section shown in Fig 1b.

Table 1: Propagation losses for hollow waveguides with different claddings and core dimensions

Core dimensions (width $\times$ height) [in wavelengths]	Number of bilayers in the cladding	propagation loss [dB/cm] - Si/SiO <sub>2</sub> cladding	propagation loss [dB/cm] - Si/Si <sub>3</sub> N <sub>4</sub> cladding
$2\lambda \times 2\lambda$	4	4.78	11.14
$2\lambda \times 2\lambda$	5	2.41	3.59
$3\lambda \times 3\lambda$	4	0.66	1.81
$3\lambda \times 3\lambda$	5	0.17	1.54
$4\lambda \times 4\lambda$	4	0.06	0.74

In our further analysis, we have again used a 3-D beam propagation method to calculate propagation losses in the waveguides with such an air gap. Specifically, we have chosen waveguides with the core dimensions of  $2\lambda \times 2\lambda$ ,  $3\lambda \times 3\lambda$ , and  $4\lambda \times 4\lambda$  where the wavelength was once again  $3.39\ \mu\text{m}$ . Results are shown in Fig 2. It can be seen that the propagation losses increase for larger gaps, as expected. It can be also seen that the core dimensions have even greater impact on propagation losses than the overall number of bilayers in the cladding (Fig 2b). This is consistent with the results reported for ARROW hollow core waveguides [9]. The core dimension of  $4\lambda \times 4\lambda$  is a good compromise between the waveguide dimensions, number of bilayers and propagation loss. The waveguide with Si/SiO<sub>2</sub> Bragg reflector has lower loss than the one with Si/Si<sub>3</sub>N<sub>4</sub>. The latter, on the other hand, has wider spectral operating range of  $1.2\text{-}6.7\ \mu\text{m}$  compared to the  $1.2\text{-}3.9\ \mu\text{m}$  [7] of the former.

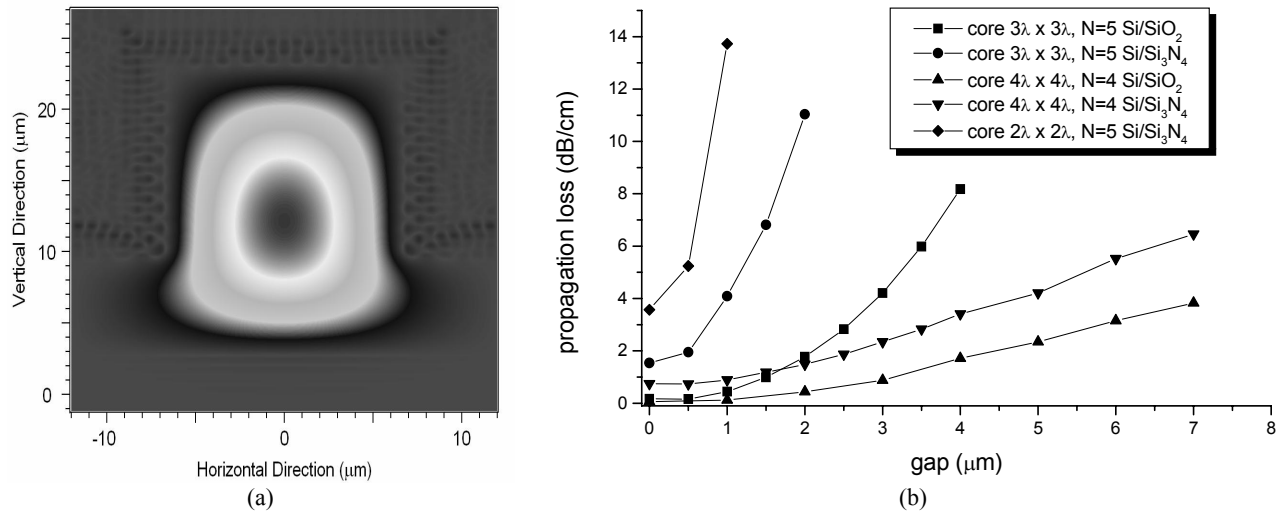


Fig. 2: (a) Mode profile for a hollow waveguide with Si/Si<sub>3</sub>N<sub>4</sub> Bragg reflectors and a gap between the two reflectors; (b) Propagation loss of hollow waveguides with Si/SiO<sub>2</sub> and Si/Si<sub>3</sub>N<sub>4</sub> Bragg reflectors as a function of the gap between the two claddings

### 3. SLOT WAVEGUIDES

When two Si-wires are very close to each other, it is possible to realise another guiding structure, usually known as the slot waveguide [12]. In this structure, the guided light is strongly confined in a narrow low-index gap between two high-index photonic wires (Fig. 3). Slot waveguides have been analysed in detail at telecommunication wavelengths [e.g. 13, 14, 15] and in this paper we have calculated the confinement factor in the slot, the effective index and the sensitivity to the slot refractive index change at the wavelength of 3.39  $\mu\text{m}$ . We have used the same FEM approach as in [16].

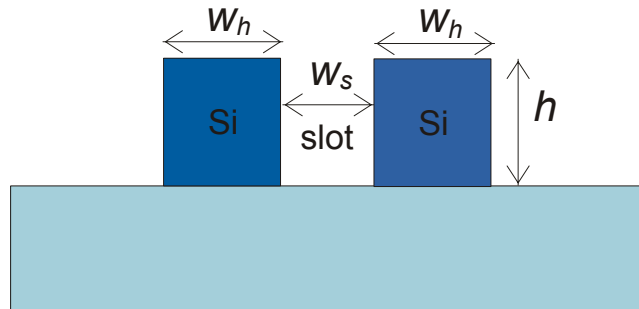


Fig. 3: Schematic of the slot waveguide

In Fig. 4a, the effective index of the quasi-TE mode is shown as a function of the silicon wire width  $w_h$ , demonstrating an increase of the confinement factor with the increase of the slot height, as expected. The slot width is fixed at  $w_s = 400$  nm and the cover is air. An optimal condition for maximising the confinement factor can be found for specific silicon wire width and height (vertical sidewalls are assumed). This optimal wire width is of the same order as the slot width. For example, for the waveguide height of  $h = 960$  nm, the Si-wire width is  $w_h = 450$  nm, which is comparable with the gap width  $w_s = 400$  nm. This certainly eases fabrication requirements compared to those at the wavelength of 1550 nm [17]. It should be noted, that the confinement factor of the quasi-TE mode is significantly higher than the confinement factor of the quasi-TM mode, similarly to the situation at 1550 nm, hence only the quasi-TE mode is analysed in this work.

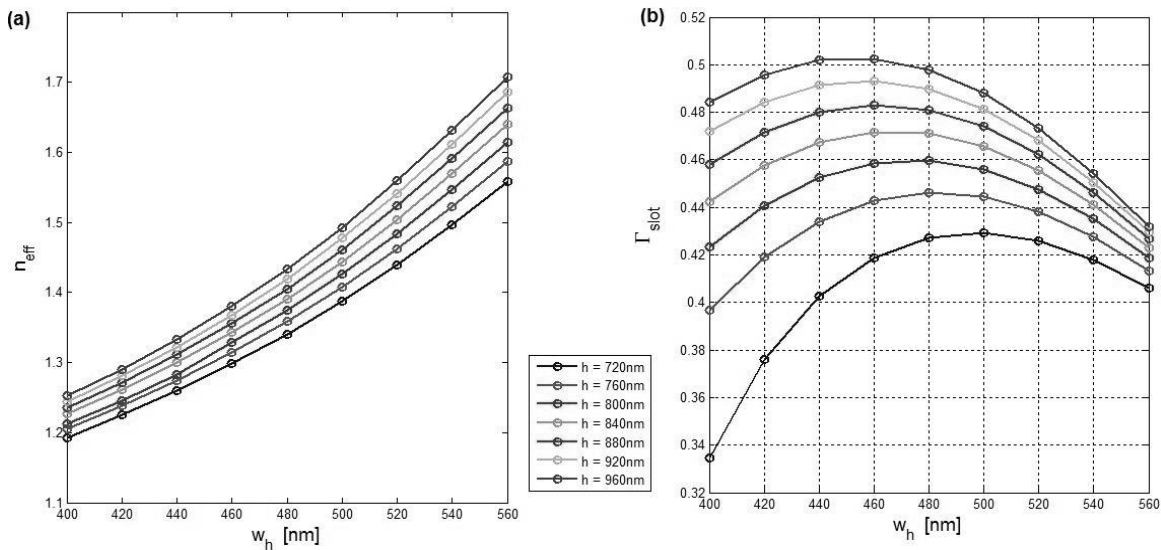


Fig. 4: (a) The effective index and (b) the slot confinement factor for the quasi-TE mode in the slot with air cover as a function of the silicon wire width  $w_h$  and height  $h$  (slot width  $w_s = 400$ nm)

By increasing the slot width, the quasi-TE mode becomes less confined in the slot and the confinement factor drops, as shown in Fig. 5a, where the maximum confinement factor is calculated as a function of the slot width for three different

waveguide heights (700, 800 and 900 nm). Finally, Fig. 5(b) shows the sensitivity of the slot waveguide, defined as  $\partial n_{eff}/\partial n_c$ , where  $n_{eff}$  is the propagating mode effective index and  $n_c$  is the cover refractive index [18], as a function of the silicon wire width, for various slot heights. As a general rule, the wire width should be similar to the slot width to have a good mode confinement in the slot region and consequently a high sensitivity. The sensitivity higher than 1 can be achieved in these structures at the mid-infrared, similarly to structures designed for near infrared wavelengths [16]. The sensitivity of the slot waveguide is by 70% larger than in a standard silicon wire waveguide. Also, the higher the slot waveguide the larger the slot area, and consequently the larger the sensitivity to the cover index change (Fig 5b).

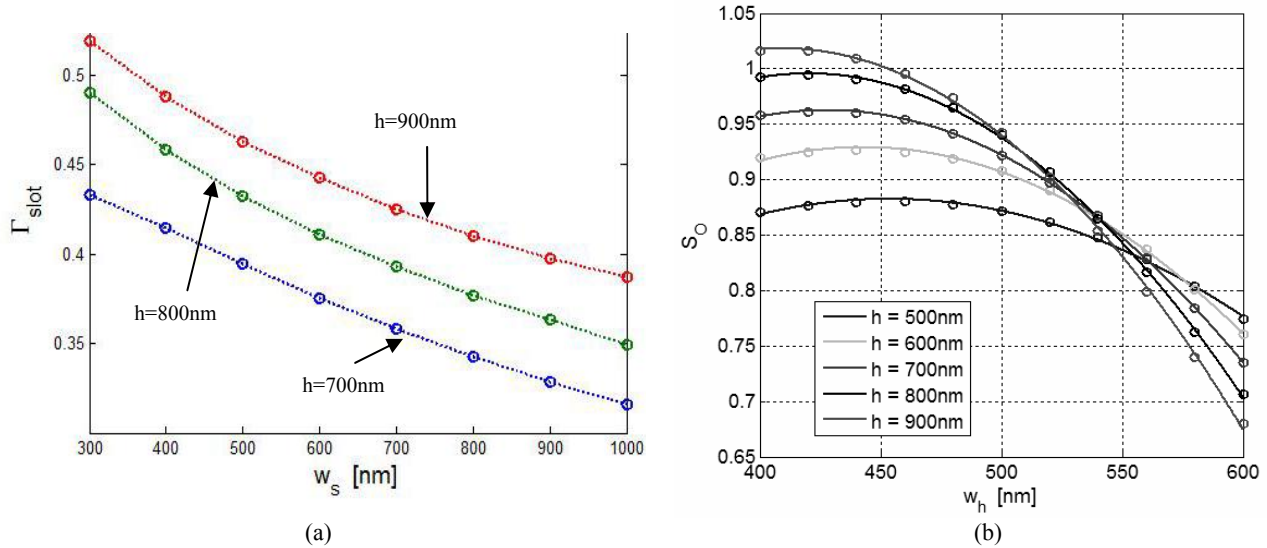


Fig. 5: (a) Maximum confinement factor of quasi-TE mode as a function of slot width  $w_s$  and height  $h$  for an air cover; (b) Sensitivity to the slot refractive index change versus wire width  $w_h$  and for different heights  $h$  ( $w_s=400$  nm)

#### 4. WAVEGUIDES WITH AIR OR POROUS SILICON CLADDINGS

Silicon waveguides with an air or a porous silicon (PSi) cladding are very attractive for mid- and long-IR applications as they would have a high transmittance in the wavelength ranges of 1.2-9 and 23-200  $\mu\text{m}$  [7]. We have already reported propagation loss measurements of a free standing waveguide structure [19] shown in Fig 6a, fabricated by the proton beam writing. To fabricate the free standing waveguides two different ion energies are required, one for the waveguide formation and the other for the pillars formation. In this section, we report a novel structure fabricated by the proton beam writing using only one ion energy.

A highly focused beam of protons of 250 keV is irradiated into a 0.7  $\Omega\cdot\text{cm}$  resistivity p-type silicon with a beam current of about 10 pA and a spot size of  $\sim 200$  nm. Such irradiation increases the local resistivity of the material and reduces the free-carrier density [20]. During subsequent electrochemical etching process, in a solution of hydrofluoric acid (48%) and ethanol with a ratio of 1:1 at a current density of 5  $\text{mA}/\text{cm}^2$  for 20 min, these defects act to trap holes from migrating to the silicon/electrolyte surface, slowing down the rate of PSi formation in the irradiated regions. As the sample is etched beyond the depth of the ion range, the structure starts to become undercut due to the isotropic etching, producing a silicon core that is surrounded by PSi (Fig 6b). After etching, the sample was rinsed in ethanol and water for about 5 min. This process has already been successfully used for microfabrication of complex free-standing structures in silicon by subsequently removing the PSi layer [21, 19]. The attractiveness of using the PSi is that the thickness and refractive index of PSi can be tuned over a wide range (1.2-3.0) by controlling the etching parameters [22].

Prior to the measurement of the propagation loss at 1550 nm, the samples were annealed at 500°C for 2 hours in inert argon atmosphere. According to Day et. al., [23] temperatures of 400-450°C are sufficient to anneal out more than 90% of the defects caused by the proton irradiation of silicon. The propagation loss of  $6.7 \pm 0.8$  dB/cm and  $6.8 \pm 0.7$  dB/cm has been measured for TE and TM polarization, respectively. These losses are significantly smaller compared to the value of  $\sim 20$  dB/cm typically measured before annealing. The main source of the propagation loss in the annealed waveguides is the surface roughness. Also, the irradiation process influences the sidewall morphology of the waveguide due to beam intensity fluctuations from the accelerator [24], beam resolution and stage scanning speed [25]. We are currently investigating a possibility to reduce the surface roughness by using different etching conditions and scanning parameters, as well as post-fabrication treatment such as oxidation.

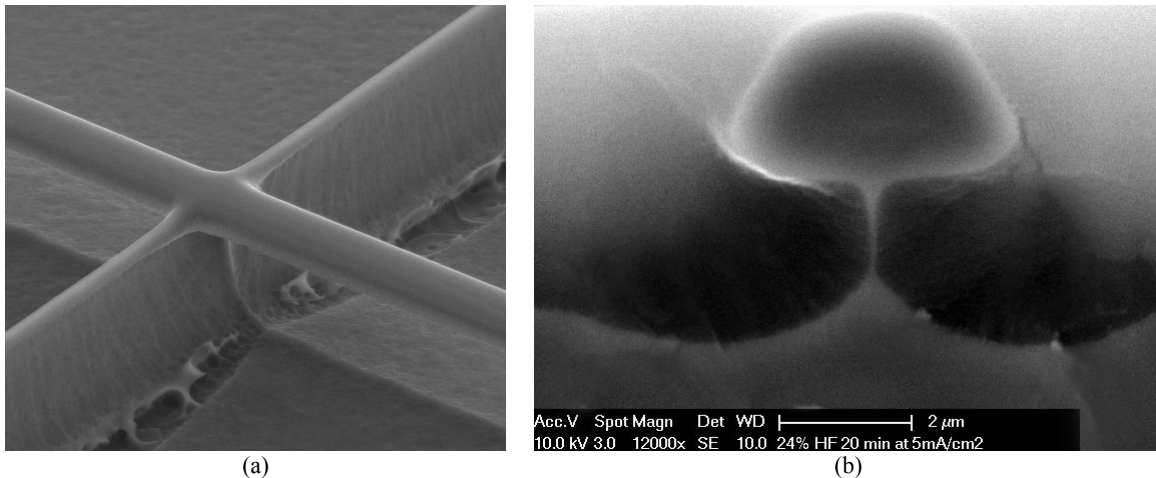


Fig. 6: a) SEM micrograph of a free-standing waveguide b) cross sectional SEM view of a waveguide with porous Si cladding

## 5. CONCLUSION

In this paper we have presented three different waveguide structures that can find applications in the mid-infrared wavelength range. We have shown that in order to reduce the propagation loss of the hollow core waveguides, the core dimensions should be at least  $4\lambda \times 4\lambda$ , where  $\lambda$  is the operating wavelength. We have also shown that the fabrication requirements for slot waveguides, that are also interesting for sensing applications in the mid-infrared region, are much more relaxed compared to the near-infrared, and therefore state of the art facilities are not required. Finally, we have reported the fabrication and propagation loss measurements of the silicon / porous silicon waveguide that is transparent in both mid- and long-infrared region. The propagation loss of  $\sim 7$  dB/cm has been measured at 1550 nm after annealing at 500°C. Further work is underway to reduce the loss by the modification of the fabrication process.

## ACKNOWLEDGEMENTS

This work was partly funded by the Royal Society UK project 2006-R2/IJP.

## REFERENCES

- 
- [1] A. Krier (Ed.), *Mid-infrared semiconductor optoelectronics*, Springer-Verlag, London, 2006.
  - [2] Q. Yang et al., *Appl. Phys. Lett.*, **88**, 121127 (2006).
  - [3] M. Graf et al., *Appl. Phys. Lett.*, **88**, 241118 (2006).
  - [4] M. Razeghi et al., *Proc. 8<sup>th</sup> Int. Conf. Mid-infrared Optoelectron.*, May 2007, Bad Ischl, Austria, p. 36.

- 
- [5] G. J. Hawkins, *PhD thesis*, University of Reading, UK, 1998.
- [6] E. D. Palik, *Handbook of optical constants of solids vol 1*, Academic: New York.
- [7] R. A. Soref, S. J. Emelett and W. R. Buchwald, *J. Opt. A: Pure Appl. Opt.* **8**, 840 (2006).
- [8] V. Raghunathan, D. Borlaug, R. R. Rice, and B. Jalali, *Opt. Express*, **15**, 14355 (2007).
- [9] R. Bernini et al., *IEEE J. Sel. Top. Quantum Electron.*, **8**, 106 (2002).
- [10] H. Schmidt et al., *IEEE J. Sel. Top. Quantum Electron.*, **11**, 519 (2005).
- [11] [www.rsoftdesign.com](http://www.rsoftdesign.com)
- [12] Q. Xu, V. R. Almeida, R. R. Panepucci, and M. Lipson, *Opt. Lett.* **29**, 1626 (2004).
- [13] T. Baehr-Jones et al., *Opt. Express*, **13**, 5216 (2005).
- [14] C. A. Barrios and M. Lipson, *Opt. Express*, **13**, 10092 (2005).
- [15] P. Mullner and R. Hainberger, *IEEE Photon. Technol. Lett.*, **18**, 2557 (2006).
- [16] F. Dell'Olivo and V. M. N. Passaro, *Opt. Express*, **15**, 4977 (2007).
- [17] J.-M. Fedeli et al., *Group IV Photonics*, 19-21 September 2007, Tokyo, Japan, ThC3.
- [18] O. Parriaux and G. J. Valdhuis, *J. Lightwave Technol.*, **16**, 573 (1998).
- [19] P. Y. Yang et al., *Appl. Phys. Lett.*, **90**, 241109 (2007).
- [20] M. B. H. Breese et al., *Phys. Rev. B*, **73**, 035428 (2006).
- [21] E. J. Teo et al., *Appl. Phys. Lett.*, **84**, 3202 (2004).
- [22] F. Watt et al., *Nucl. Instrum. Meth. Phys. Res. B*, **210**, 14 (2003).
- [23] A. C. Day, W. E. Horne, and I. Arimura, *IEEE Trans. Nucl. Sci.*, **27**, 1665 (1980).
- [24] E. J. Teo et al., *J. Vac. Sci. Technol. B*, **22**, 560 (2004).
- [25] T. C. Sum et al., *Appl. Phys. Lett.*, **85**, 1398 (2004).